Fully Integrated Silicon Probes for High-Density Recording of Neural Activity

James J. Jun[1*], Nicholas A. Steinmetz[2,3,4*], Joshua H. Siegle[5*], Daniel J. Denman[5*], Marius Bauza[6,7*], Brian Barbarits[1*], Albert K. Lee[1*], Costas A. Anastassiou[5], Alexandru Andrei[8], Çağatay Aydın[9,10], Mladen Barbic[1], Timothy J. Blanche[5,11], Vincent Bonin[8,9,10,12], João Couto[9,10], Barundeb Dutta[8], Sergey L. Gratiy[5], Diego A. Gutnisky[1], Michael Häusser[3,13], Bill Karsh[1], Peter Ledochowitsch[5], Carolina Mora Lopez[8], Catalin Mitelut[5], Silke Musa[8], , Michael Okun[2,3,14], Marius Pachitariu[2,3], Jan Putzeys[8], P. Dylan Rich[1], Cyrille Rossant[2,3], Wei-lung Sun[1], Karel Svoboda[1], Matteo Carandini[4], Kenneth D. Harris[2,3], Christof Koch[5], John O'Keefe[6,7], Timothy D. Harris[1]†

[1]HHMI Janelia Research Campus, 19700 Helix Dr., Ashburn, VA 20147
[2]UCL Institute of Neurology, University College London, London WC1N 3BG, UK
[3] Department of Neuroscience, Physiology and Pharmacology, University College London, London WC1E 6DE, UK
[4]UCL Institute of Ophthalmology, University College London, London EC1V 9EL, UK
[5]Allen Institute for Brain Science, 615 Westlake Ave N, Seattle, WA 98109
[6]Department of Cell and Developmental Biology, University College London, London WC1E 6BT, UK
[7]Sainsbury Wellcome Center, University College London, London W1T 4JG, UK
[8]imec, Kapeldreef 75, 3001 Heverlee, Leuven Belgium
[9]Neuro-Electronics Research Flanders, Kapeldreef 75, 3001 Leuven Belgium
[10]KU Leuven, Department of Biology, Naamsestraat 59, 3000 Leuven, Belgium
[11]White Matter LLC, Seattle, USA
[12]VIB, 3001 Leuven, Belgium
[13]Wolfson Institute for Biomedical Research, University College London, Gower Street, London WC1E 6BT, UK
[14]Centre for Systems Neuroscience, University of Leicester, Leicester LE1 7QR, UK

Summary Paragraph

Sensory, motor, and cognitive operations involve the coordinated action of large neuronal populations across multiple brain regions in both superficial and deep structures[1,2]. Existing extracellular probes record neural activity with excellent spatial and temporal (sub-millisecond) resolution but from only a few dozen neurons per shank. Optical Ca^{2+} imaging[3–5] offers more coverage but lacks the temporal resolution to reliably distinguish individual spikes and does not measure local field potentials. To date, no technology compatible with unrestrained animals has combined high spatiotemporal resolution with large volume coverage. To satisfy this need, we

designed, fabricated, and tested a new silicon probe called *Neuropixels*. Each probe has 384 recording channels that can programmably address 960 CMOS processing-compatible low-impedance TiN[6] sites that tile a single 10 mm long, 70x20 µm cross section shank. The 6x9 mm probe base is fabricated with the shank on a single chip. Voltage signals are filtered, amplified, multiplexed, and digitized on the base, allowing noise-free digital data transmission directly from the probe. The combination of dense recording sites and high channel count yielded well-isolated spiking activity from hundreds of neurons per probe implanted in mice and rats. Using two probes, more than 700 well-isolated single neurons were simultaneously recorded from five brain structures in an awake mouse. The fully integrated functionality and small size of *Neuropixels* probes allowed recording large populations of neurons from multiple brain structures in freely moving animals. This combination of high-performance electrode technology and scalable chip fabrication methods opens the path to record brain-wide neural activity during behavior.

Historically, the most widely employed tool for recording neuronal activity has been the extracellular microelectrode[7]. To make further progress in understanding the coordinated activity underlying brain computations, it is critical to increase the number of single neurons that can be simultaneously monitored[8–10]. This requires large dense arrays of recording sites, ideally compatible with freely-moving rodents. To this end, with the support of the Howard Hughes Medical Institute's Janelia Research Campus, Allen Institute for Brain Science, Gatsby Charitable Foundation, and Wellcome Trust, we designed, fabricated, and tested a new class of silicon probes[11].

Neuropixels probes were developed in three phases with seven design goals. The first two goals were: (i) dense and extensive recording sites to isolate individual neurons across large regions of the brain[12], and (ii) small cross-sectional area to minimize brain tissue damage. We achieved these two goals using a custom 130 nm CMOS fabrication process[13]. This process allowed us to place 960 sites on a single, 10 mm long, non-tapered shank with 70x20 µm cross section. This site count on a single shank is a large improvement over existing multi-shank silicon probes[14–16].

We chose to focus on maximizing site count and minimizing width for a single shank because it presented the most essential engineering challenges. The solutions can be extended in a straightforward manner to multiple shanks for transverse coverage. The 12x12 μm sites are arranged in a checkerboard pattern with 4 columns and 25 μm center to center nearest neighbor spacing (Figure 1a,b). *Neuropixels* probes feature user-programmable switches that allow recording channels to simultaneously address 384 of the 960 total sites. We found no performance loss for switchable sites compared to a test version of the probe with unswitchable sites (Extended Data Figure 1a,b).

We further sought to develop probes with (iii) low noise, (iv) resistance to movement artifacts or other interference, and (v) efficient data transmission by integrating low noise analog amplifiers, multiplexers, and digitizers into the probe base. This integration enables small size, minimal weight, noise immunity, and a digital data output stream transmitted via a single thin cable. The 6x9 mm base, fabricated with the same CMOS processes used for the shank, yielded a finished probe ~250 mg in weight, small enough for chronic implants in mice (Figure 1c). We used 10-bit analog-to-digital converters to minimize base area and power consumption. Because 10 bits do not provide sufficient resolution for wideband recording, the continuous data stream from each channel was split into action potential (AP, 0.3-10 kHz) and local field potential (LFP, 0.5-1000 Hz) bands which were separately amplified and digitized (AP, 30 kHz; LFP, 2.5 kHz). Together with low impedance TiN sites (see below) this system achieves uniform low noise (AP band ~5 μV root-mean-squared (RMS) Figure 1d; LFP band ~9 μV RMS; Extended Data Table 1, Options 1 and 3). We explored the use of on-site amplifiers (buffer amplifiers under each site) but found no advantage in performance (Extended Data Figures 1c-f and 2). Furthermore, such active probes had increased noise (Extended Data Table 1) and light sensitivity (Extended Data Figure 3a,b).

Finally, we sought to (vi) enable long-term recording stability and (vii) ensure low-cost scalable fabrication. As a key element for stability and scalable fabrication, we developed porous TiN[6] for

the recording site material. Sites made of this material are compatible with CMOS processing and feature low, uniform impedance (149 ± 6 kOhm, Figure 1e). Our criterion for long-term stability was good performance out to eight weeks post-implant, a time frame chosen to ensure that most research questions in rodents, our focus for these probes, can be addressed. We found no stability difference between TiN and standard (PEDOT[17]-coated gold) site probes implanted in rat neocortex (Extended Data Figure 4a-d). Furthermore, probes with and without on-site amplifiers, and with and without switchable sites, all exhibited stable firing rates in rat medial prefrontal cortex (mPFC) (Extended Data Figures 4e-g and 5). The use of high-throughput silicon fabrication processes to achieve our first six objectives also ensured that *Neuropixels* probes can be manufactured at low cost and large scale.

Neuropixels probes allowed us to obtain electrophysiological measurements across a large spatial extent with an unprecedented level of detail. In one example, a probe was inserted into the brain of an awake, head-fixed mouse, targeting primary visual cortex (V1) and the lateral posterior (LP) nucleus of the thalamus, which receives direct projections from V1[18]. Because the probes record activity with the same spatial resolution along the entire shank, the data can be conveniently displayed as images with each site represented as a "pixel." Using these images, structural boundaries can be visualized using simple measures of neural activity, such as multi-unit firing rates or signal amplitude in certain frequency ranges (Figure 2a-c; also see Extended Data Figure 6). From this recording (Figure 2d), 206 putative individual neurons were isolated from the cortex, hippocampus, and thalamus using automated spike sorting methods[19] with manual curation[20]. Regions near the top and bottom of the probe were strongly modulated by visual stimuli (Figure 2e). Histology revealed that these regions corresponded to V1 and LP (Figure 2f,g).

In a separate example experiment, two probes were inserted into the brain of an awake, head-fixed mouse. One probe spanned sensory cortex, hippocampus, and thalamus (Figure 3a) while the second spanned motor cortex and striatum (Figure 3b). In this experiment, we recorded 741

putative single neurons simultaneously.

Recordings with such high yields were the norm with *Neuropixels* probes, from both superficial and deep structures. To quantify single neuron isolation across experiments, we compared statistics from recordings made from multiple laboratories in diverse brain structures such as cortex, hippocampus, striatum, thalamus, superior colliculus, and cerebellum (n = 13 mice, 15 experiments). *Neuropixels* probes allowed isolation of 20-200 neurons per structure (79.0 ± 55.5 per structure, Figure 3c). The number of isolated neurons depended on the number of sites in that region (0.64 ± 0.32 neurons per site, Figure 3d) and the spatial spread of each neuron's waveform on the probe. Although most sites sampled signals from multiple (6.9 ± 5.1) neurons (Figure 3e), good single-neuron isolation was possible because each neuron was visible across 9.5 ± 5.3 sites (Figure 3e, Extended Data Figure 7a,b). A neuron appearing on 4-6 sites enables effective sorting[12]. *Neuropixels* probes maintained high signal quality across >10 acute insertions (Extended Data Figure 7c,d).

Since light induces voltage transients in nearly all materials used for extracellular electrophysiology, we tested the sensitivity of *Neuropixels* probes to optical excitation conditions used for optogenetic perturbations in tandem with extracellular electrophysiology[21]. Direct illumination of the probes in saline resulted in a small, non-saturating artifact which can be minimized using sinusoidal or ramped light pulses (Extended Data Figure 3c-e) or subtracted out. We were thus able to combine *Neuropixels* recording with optogenetic stimulation of both excitatory and inhibitory neuron populations *in vivo* (Extended Data Figure 8).

A variety of experiments benefit from chronic implantation of silicon probes and recording in freely moving rodents[22,23]. Due to their light weight, small footprint, and integrated electronics, *Neuropixels* probes are ideal for such recordings. While there is a prior report of silicon probe recordings with >300 isolated neurons[16], this yield was achieved with a 16-shank array coupled to external amplification and multiplexing electronics requiring large-form-factor hardware, making it impractical to use the probes in freely moving rodents. We monitored activity for at

least 8 weeks in a variety of chronic implant geometries. Not only is this sufficient time for most rodent studies, but onset of activity loss is usually observed within this time frame[24].

We tested chronic implants of *Neuropixels* probes and obtained large scale single-neuron recordings in both freely-moving rats (Figure 4 and Extended Data Figure 5) and head-fixed mice (Extended Data Figure 9). For example, a probe implanted in rat entorhinal cortex isolated the activity of 127 neurons, including 22 grid cells[25], 49 days after implantation (Figure 4a-c). Similarly, a probe implanted in rat mPFC delivered low-noise recordings of hundreds of neurons (isolated using another recently developed spike sorting package[26]) simultaneously for more than 8 weeks (Figure 4d-g and Extended Data Figure 5), and a probe implanted in the mouse frontal cortex and lateral septal nucleus delivered stable chronic recordings of more than 100 neurons over >150 days (Extended Data Figure 9b). Across 14 chronic implants in rat mPFC, we did not observe degradation of spiking activity over 8 weeks (linear regression t-test, single-tailed, $p>0.1$). We have yet to find specific limits to the duration of chronic recordings with *Neuropixels* and saw no sign that the probes themselves deteriorate (Figures 4g and Extended Data Figures 5 and 9).

In summary, *Neuropixels* probes provide an order of magnitude increase in the number of simultaneously recorded neurons obtainable per shank while maintaining low noise. This expanded recording capability has many applications, such as simultaneously monitoring the inputs and outputs of diverse regions (e.g. by recording populations in thalamus simultaneously with a target cortical area), as well as assessing the relationship of behavior to activity distributed across the brain. Moreover, due to the integrated circuitry for amplification, multiplexing and digitization, *Neuropixels* probes have a small physical footprint and minimal cabling, important for studying unrestrained behaviors, and require only a simple interface board to acquire data. More generally, such integration realizes the promise of fully combining advanced, scalable chip fabrication methods with electrode technology. The 1 cm recording length — comparable to the size of the rodent brain — enables recording from multiple brain regions simultaneously at

neuronal scale and with high temporal resolution, an essential step toward understanding the global coordination of activity fundamental to brain function[27–29].

Acknowledgments

We thank the support of the charities that fully funded this work: HHMI Janelia Research Campus, Allen Institute for Brain Science, Gatsby Charitable Foundation (grant GAT3353), and the Wellcome Trust (grant 100154). We thank Sarah Caddick for early and continued enthusiastic support of the project. We thank György Buzsáki for initial discussions on design choices and testing strategies. CM, SLG and CAA would like to thank NSG portal personnel for offering core-hour access to the San Diego supercomputing facility, troubleshooting and support. The Allen Institute for Brain Science wishes to thank the enduring support of our founders, Paul G. Allen and Jody Allen, without whom this work could not have been accomplished. JC, CA and VB were funded by NERF. Experiments and software development in the laboratory of MC and KDH were supported by the Wellcome Trust (095668, and 095669). NAS was supported by postdoctoral fellowships from the Human Frontier Sciences Program and the Marie Curie Actions of the EU.

Author Contributions: AKL, TDH, and BD conceived and originated the project. TDH, CK, JO, MC, KDH, MH, AKL, and KS Secured project funding. TDH, AKL, BD, SM, CML, JP, JO, CK, TJB, JJJ, NAS, JHS, DJD, MB1, BB, DAG, KDH, BK, PL, PDR, and KS Determined specifications. AA, CML, SM, JP, WS, and TDH Designed and produced devices and firmware. JJJ, NAS, JHS, DJD, BB, TJB, BK, PL, CML, SM, JP, WS and TDH Tested devices in vitro. NAS, JHS, DJD, MB2, VB, CA, and JC Performed acute recordings in mouse or rat. JJJ and PDR Performed chronic recordings in rat mPFC. MB1 Performed chronic recordings in rat EC. NAS and MO Performed chronic recordings in mouse. JJJ, NAS, JHS, MB1, BB, TJB, CML, SM, JP, and WS Developed instrumentation or other materials. JJJ, NAS, JHS, DJD, MB1, BB, AKL, MB2, TJB, VB, MC, JC, DAG, KDH, PL, JO, MO, PDR, KS and TDH Designed experiments. BK, JP, JHS, DJD, JJJ, MP, KDH, and CR Wrote software for data acquisition or analysis. CAA, SLG, and CM Performed simulations. JJJ, NAS, JHS, DJD, MB1, BB, CA, and JC analyzed data. TDH, AKL, MC, NAS, DJD, CK, JJJ, JHS, MB1, VB, JC, KDH, CML, BD, and JO Wrote and edited the manuscript with input from all authors. JJJ, NAS, JHS, DJD, MB1, BB and, JC Prepared figures. TDH,

BD, MC, JO, TJB, KDH, DJD, VB, CK, and KS Supervised work. TDH and SM Managed the project.

Author Information: reprints and Permissions information is available at Nature.com/reprints. The authors declare no competing financial interests. Correspondence and requests for materials or data should be addressed to TDH (harrist@janelia.hhmi.org).

References

1. Lewis, C. M., Bosman, C. A. & Fries, P. Recording of brain activity across spatial scales. *Curr. Opin. Neurobiol.* **32,** 68–77 (2015).
2. Bargmann, C. *et al.* BRAIN 2025: a scientific vision. *Brain Research Through Advancing Innovative Neurotechnologies (BRAIN) Working Group Report to the Advisory Committee to the Director, NIH. Available online at: http://www. nih. gov/science/brain/2025/(US National Institutes of Health, 2014)* (2014).
3. Sofroniew, N. J., Flickinger, D., King, J. & Svoboda, K. A large field of view two-photon mesoscope with subcellular resolution for in vivo imaging. *Elife* **5,** (2016).
4. Hamel, E. J. O., Grewe, B. F., Parker, J. G. & Schnitzer, M. J. Cellular level brain imaging in behaving mammals: an engineering approach. *Neuron* **86,** 140–159 (2015).
5. Ahrens, M. B., Orger, M. B., Robson, D. N., Li, J. M. & Keller, P. J. Whole-brain functional imaging at cellular resolution using light-sheet microscopy. *Nat. Methods* **10,** 413–420 (2013).
6. Musa, S. Titanium Nitride Electrode. US Patent 9,384,990 filed 17 Nov. 2014, and issued 5 Jul. 2016
7. Buzsaki, G. Large-scale recording of neuronal ensembles. *Nat. Neurosci.* **7,** 446–451 (2004).
8. Stevenson, I. H. & Kording, K. P. How advances in neural recording affect data analysis. *Nat.*

Neurosci. **14,** 139–142 (2011).

9. Meister, M., Wong, R. O. L., Baylor, D. A. & Shatz, C. J. Synchronous bursts of action potentials in ganglion cells of the developing mammalian retina. *Science* **252,** 939–944 (1991).
10. Wilson, M. A. & McNaughton, B. L. Dynamics of the hippocampal ensemble code for space. *Science* **261,** 1055–1058 (1993).
11. Seymour, J. P., Wu, F., Wise, K. D. & Yoon, E. State-of-the-art MEMS and microsystem tools for brain research. *Microsystems & Nanoengineering* **3,** micronano201666 (2017).
12. Harris, K. D., Henze, D. A., Csicsvari, J., Hirase, H. & Buzsaki, G. Accuracy of tetrode spike separation as determined by simultaneous intracellular and extracellular measurements. *J. Neurophysiol.* **84,** 401–414 (2000).
13. Mora Lopez, C. *et al.* A neural probe with up to 966 electrodes and up to 384 configurable channels in 0.13 μm SOI CMOS. *IEEE Trans. Biomed. Circuits Syst.* (2017).
14. Scholvin, J. *et al.* Close-Packed Silicon Microelectrodes for Scalable Spatially Oversampled Neural Recording. *IEEE Trans. Biomed. Eng.* **63,** 120–130 (2016).
15. Rios, G., Lubenov, E. V., Chi, D., Roukes, M. L. & Siapas, A. G. Nanofabricated Neural Probes for Dense 3-D Recordings of Brain Activity. *Nano Lett.* (2016). doi:10.1021/acs.nanolett.6b02673
16. Shobe, J. L., Claar, L. D., Parhami, S., Bakhurin, K. I. & Masmanidis, S. C. Brain activity mapping at multiple scales with silicon microprobes containing 1,024 electrodes. *J. Neurophysiol.* **114,** 2043–2052 (2015).
17. Ludwig, K. A. *et al.* Poly(3,4-ethylenedioxythiophene) (PEDOT) polymer coatings facilitate smaller neural recording electrodes. *J. Neural Eng.* **8,** 014001 (2011).
18. Roth, M. M. *et al.* Thalamic nuclei convey diverse contextual information to layer 1 of visual cortex.

Nat. Neurosci. **19,** 299–307 (2016).

19. Pachitariu, M., Steinmetz, N. A., Kadir, S. N., Carandini, M. & Harris, K. D. Fast and accurate spike sorting of high-channel count probes with KiloSort. in *Advances In Neural Information Processing Systems* 4448–4456 (2016).
20. Rossant, C. *et al.* Spike sorting for large, dense electrode arrays. *Nat. Neurosci.* **19,** 634–641 (2016).
21. Yizhar, O., Fenno, L. E., Davidson, T. J., Mogri, M. & Deisseroth, K. Optogenetics in neural systems. *Neuron* **71,** 9–34 (2011).
22. Wang, Y., Romani, S., Lustig, B., Leonardo, A. & Pastalkova, E. Theta sequences are essential for internally generated hippocampal firing fields. *Nat. Neurosci.* **18,** 282–288 (2015).
23. Buzsáki, G., Horváth, Z., Urioste, R., Hetke, J. & Wise, K. High-frequency network oscillation in the hippocampus. *Science* **256,** 1025–1027 (1992).
24. Karumbaiah, L. *et al.* Relationship between intracortical electrode design and chronic recording function. *Biomaterials* **34,** 8061–8074 (2013).
25. Hafting, T., Fyhn, M., Molden, S., Moser, M.-B. & Moser, E. I. Microstructure of a spatial map in the entorhinal cortex. *Nature* **436,** 801–806 (2005).
26. Jun, J. J. *et al.* Real-time spike sorting platform for high-density extracellular probes with ground-truth validation and drift correction. *bioRxiv* 101030 (2017). doi:10.1101/101030
27. Harris, K. D. Neural signatures of cell assembly organization. *Nat. Rev. Neurosci.* **6,** 399–407 (2005).
28. Churchland, M. M., Yu, B. M., Sahani, M. & Shenoy, K. V. Techniques for extracting single-trial activity patterns from large-scale neural recordings. *Curr. Opin. Neurobiol.* **17,** 609–618 (2007).
29. Alivisatos, A. P. *et al.* The brain activity map project and the challenge of functional connectomics.

Neuron **74,** 970–974 (2012).

30. Boccara, C. N. *et al.* Grid cells in pre- and parasubiculum. *Nat. Neurosci.* **13,** 987–994 (2010).

Figure Legends

Figure 1. The *Neuropixels* probe. (a) Illustration of probe tip, showing checkerboard site layout (dark squares). **(b)** Scanning electron microscope image of probe tip. **(c)** Probe packaging, including flex cable and headstage for bidirectional data transmission. **(d)** Example of root-mean-squared (RMS) noise levels of the AP band in saline, for 384 sites (switchable option). Mean ± standard deviation = 5.1 ± 0.6 µV. **(E)** Typical site impedance in saline, for 384 sites, measured for each site with sinusoidal 1 nA injected currents at 1 kHz (see supplemental material). Mean ± standard deviation = 149 ± 6 kΩ.

Figure 2. Recording from large neuronal populations with a single probe in an awake head-fixed mouse. Signals were acquired from a *Neuropixels* probe inserted through primary visual cortex (V1), CA1 and dentate gyrus (DG) regions of the hippocampus, and the lateral posterior (LP) nucleus of the thalamus. Approximate structure boundaries are shown in gray next to probe depth scale. For the heat maps, each square represents a single site. (**a**) RMS amplitude of the AP band signal for 1 s intervals, averaged over 10 intervals. (**b**) Firing rate measured from AP band crossings of a –50 µV threshold, in a 10 s interval. (**c**) Gamma-band LFP power (35-80 Hz), computed by Welch's method in a 1 s interval, averaged over 10 intervals. (**d**) Distribution of putative single neuron locations (channel with peak amplitude), smoothed with a 1-dimensional Gaussian filter (radius = 4.5 sites). (**e**) Visual modulation index of spike activity (defined as $((X-Y)/X)^2$ where X is the 75th percentile of the PSTH and Y is the 25th percentile) in response to 20 Hz visual flicker (15 s duration), for single neurons closest to each recording site, smoothed with a 1-dimensional Gaussian filter (radius = 6 sites). Behind the heat maps are example traces from every 25th channel shown for the AP band (behind A and B) and the LFP band (behind C), along with example spike rasters for all putatively-isolated single neurons (behind D and E, during visual flicker stimulation); n=103 neurons in thalamus, 41 in hippocampus, and 62 in cortex. Vertical/horizontal scale bars: AP band (A,B), 315 µV/165 ms; LFP band (C), 1550 µV/290 ms; single neuron (D,E) 2.6 s. (**f**) Histological reconstruction of the probe track with DAPI (blue) and DiI (red), (**g**) registered to the Allen Reference Atlas.

Figure 3. Recording from multiple brain structures in awake head-fixed mice. (a,b)

Example experiment with two probes recording from 5 major brain structures. Approximate probe locations are shown overlaid on the Allen Reference Atlas at left. A total of 741 putative individual neurons were recorded simultaneously; number of putative single neurons from each structure shown in parentheses. **(c-f)** Quantification of neuron yield across 9 brain structures (n=15 recordings from 13 mice). For each recording, structure borders were annotated manually based on histological reconstruction or physiological signatures. For each structure , we computed: the total number of putative single neurons **(c)**; the efficiency of isolating single neurons (total number of neurons isolated from a structure divided by the number of sites in that structure) **(d)**; the density of neurons per site (number of neurons with median waveform maximum absolute value >20μV for each site) **(e)**; and the spread of individual neurons' waveforms across the probe (number of channels with median waveform maximum absolute value >20μV) **(f)**. Box plots show median and quartile range (whiskers = 1.5X interquartile range). Individual data points are overlaid (number of points above each plot).

Figure 4. Recordings from entorhinal and medial prefrontal cortices using chronic implants in unrestrained rats. (**a**) Schematic representation of the implant in entorhinal cortex. (**b**) Filtered voltage traces from 130 channels spanning 1.3 mm of the shank. (**c**) Rate maps and waveforms for 12 selected grid cells with a similar grid scale. Color code corresponds to anatomical location in **b**. Peak firing rate given at bottom of rate maps, grid score[30] at top. In total 127 entorhinal cells were recorded from one rat on day 49 after implantation while it freely foraged for food in a 1.8x1.0 m box. 36 neurons exhibited spatially modulated firing patterns, 22 of which passed the standard grid cell criterion (grid score above 0.27). (**d**) mPFC recording (n=3 rats), 200 ms of voltage traces and examples of waveforms from two sorted neurons. Insets: Dark lines show average waveform overlaid with 30 randomly selected single event raw waveforms of a neuron located at the top (green) and bottom (blue) of the distal most group of 384 sites (Array 1). (**e**) Anatomical targeting of the chronic implant in mPFC. Section was immuno-fluorescently labeled with IBA-1. (**f**) Photos showing a rat with a chronically implanted *Neuropixels* probe in mPFC. (**g**) Plot of total event rate (summed over 374 sites for array 1 and 156 sites for array 2) across recording sessions over 60 days. See supplemental material for details.

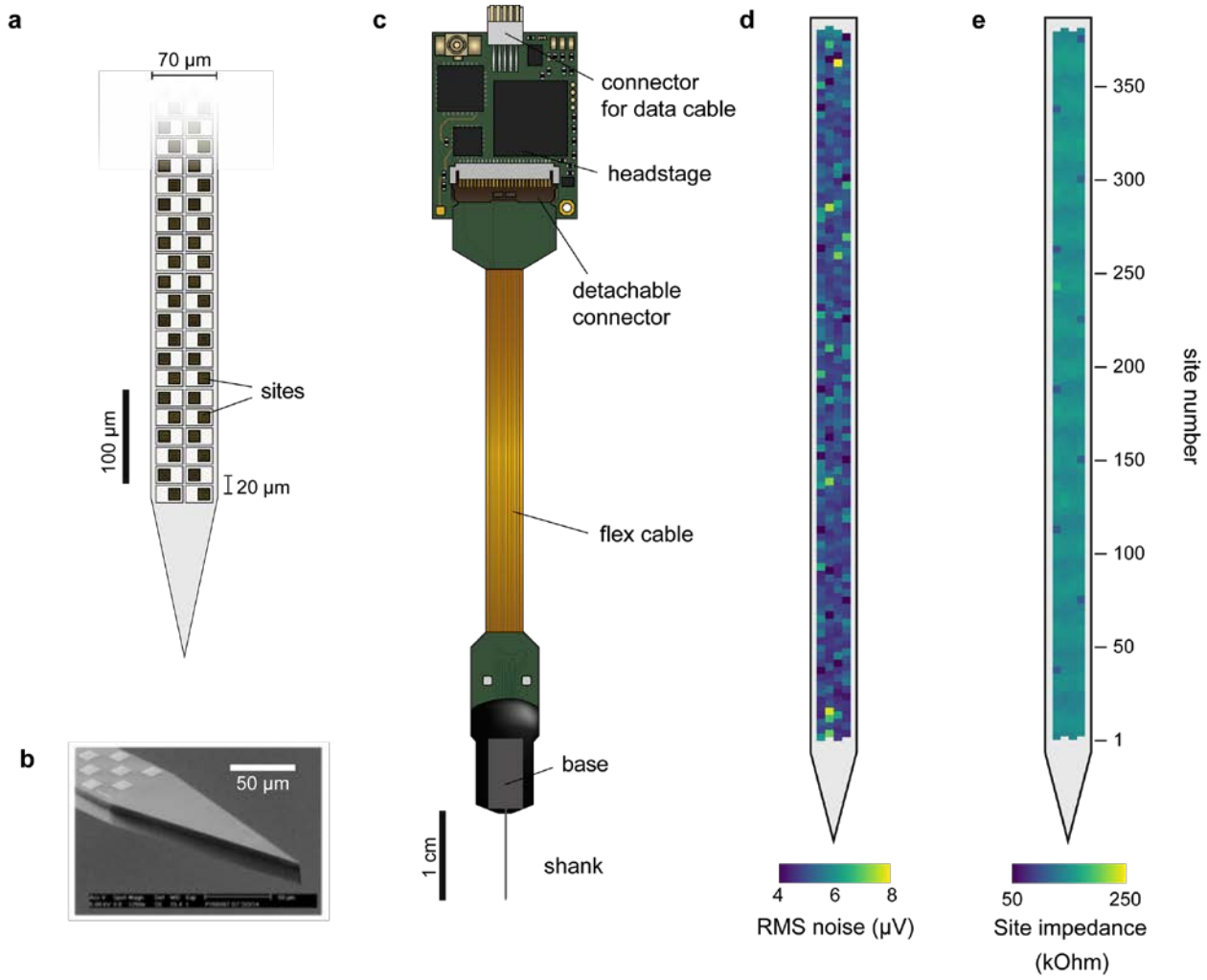
a
70 µm
sites
100 µm
20 µm
b
50 µm
c
connector
for data cable
headstage
detachable
connector
flex cable
base
shank
1 cm
d
4
6
8
RMS noise (µV)
e
350
300
250
200
150
100
50
1
site number
50
250
Site impedance
(kOhm)

Figure 1.

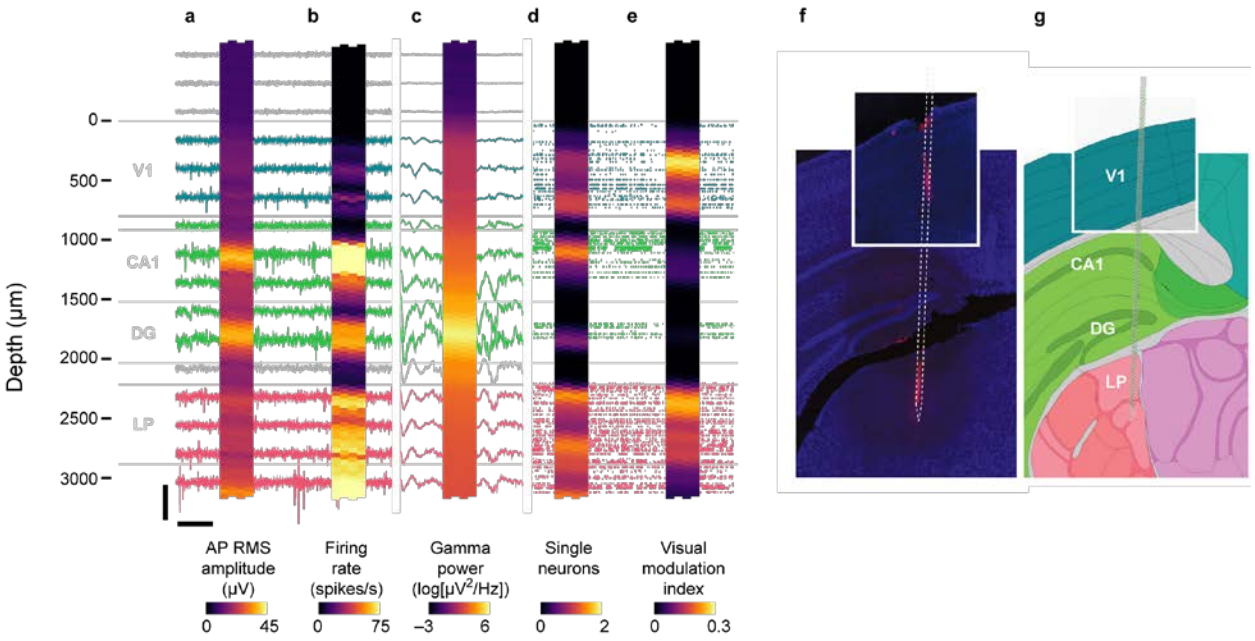
a
b
c
d
e
f
g
Depth (µm)
0
500
1000
1500
2000
2500
3000
V1
CA1
DG
LP
AP RMS amplitude (µV)
0 45
Firing rate (spikes/s)
0 75
Gamma power (log[µV²/Hz])
–3 6
Single neurons
0 2
Visual modulation index
0 0.3
V1
CA1
DG
LP

Figure 2

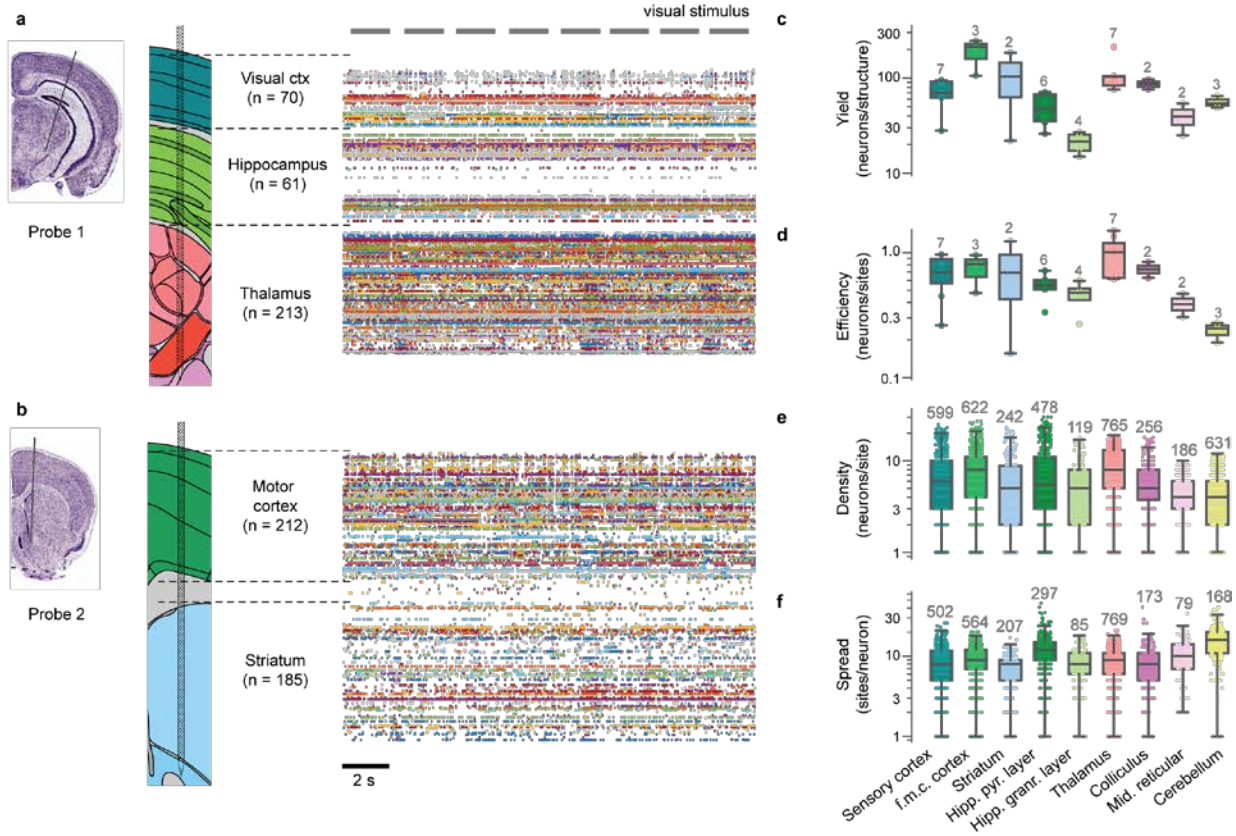
a
visual stimulus
Visual ctx
(n = 70)
Hippocampus
(n = 61)
Thalamus
(n = 213)
Probe 1
b
Motor
cortex
(n = 212)
Striatum
(n = 185)
Probe 2
2 s
c
Yield
(neurons/structure)
d
Efficiency
(neurons/sites)
e
Density
(neurons/site)
f
Spread
(sites/neuron)
Sensory cortex
f.m.c. cortex
Striatum
Hipp. pyr. layer
Hipp. granr. layer
Thalamus
Colliculus
Mid. reticular
Cerebellum

Figure 3

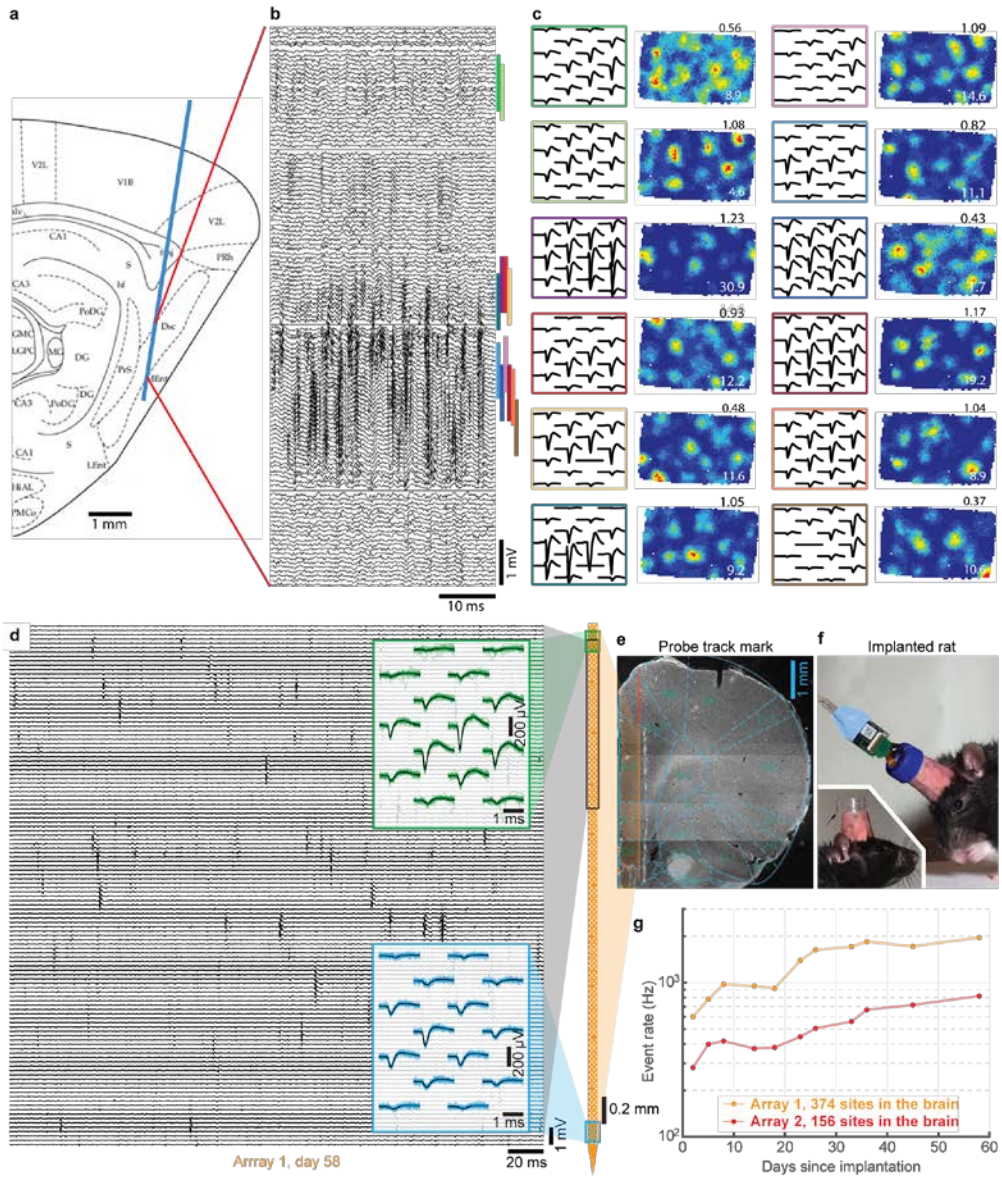
a
b
c
1 mm
10 ms
1 mV
0.56
8.9
1.09
14.6
1.08
4.6
0.82
11.1
1.23
30.9
0.43
0.93
12.2
1.17
19.2
0.48
11.6
1.04
8.9
1.05
9.2
0.37
d
200 µV
1 ms
200 µV
1 ms
1 mV
20 ms
Arrray 1, day 58
e
Probe track mark
1 mm
f
Implanted rat
g
0.2 mm
Event rate (Hz)
10^3
10^2
0
10
20
30
40
50
60
Days since implantation
Array 1, 374 sites in the brain
Array 2, 156 sites in the brain

Figure 4

Extended Data Figure Legends

Extended Data Table 1. Measured operating parameters of the 4 probe types reported in the main text (Phase 3).

Extended Data Figure 1. Comparison of switchable and active probe options. a, Cumulative distribution of the single unit peak amplitude from recordings using non-switchable (option 1, blue, n=5 recordings) or switchable (option 3, green, n=5 recordings) probes. Each distribution shows an individual recording session; sessions were spike sorted, and the mean waveform on every channel for each unit was computed. The largest absolute peak in the mean waveform on any channel was taken as the amplitude. **b,** Distribution of mean firing rate across the recording sessions for each sorted unit from non-switchable (blue, n = 119 cells) and switchable (green, n = 294 cells) probes; all recordings with each variant are combined. Switches did not have an appreciable effect on the amplitude or firing rate of recorded units. **c**, Artifacts in awake head-fixed locomoting mice are similar across passive and active probe options and can be removed by common (median) average referencing. Filtered traces (bandpass 300 to 3000 Hz) of 4 channels sampled at different depths (gray) and corrected common average referenced (CAR) traces (red). The CAR corrected traces are obtained by subtracting from each trace the median across all 120 channels (bottom). Figure panel depicts representative examples of artifacts found on both probe options. **d**, Extracellular spike waveform amplitude (signal), noise amplitude, and spike signal-to-noise ratio measured in cortex *in vivo* using passive (black) or actively amplified (red) recording sites. Voltage amplitudes are sampled from 250,000 spikes across the entire probe for each experiment (4 experiments with passive (SNR=8.78 ± 0.52, 95% confidence interval) and 4 with active (SNR=8.95 ± 0.54) recording sites). Signal-to-noise (right) distributions are similar - wilcoxon rank-sum; p-value 0.78, two-sided. **e**,**f,** Signal-to-noise ratio computed using 200,000 spikes during locomotion (red) or stationary (black) epochs. Recordings with passive sites (3 recordings) are depicted in **e** and recordings with active sites (4 recordings) in **f**. SNR distributions are similar during stationary and locomotion epochs with both probe options. Overall, the performance of probes with on-site buffer amplification is similar to that of probes with passive sites and offers no clear advantage *in vivo*.

Extended Data Figure 2. Impact and chewing transient rejection. Reduction of interfering transients with common average reference (CAR) post-processing in software. Recordings using external reference on one animal, 6 or 12 trials for each technology option. **a,** Example signal traces for a phase 3 unbuffered, switched probe in a chronically implanted rat tapped with a cable tie. Shown is the median across all 374 recording sites (red), the raw traces (gray, from 4 adjacent sites), and traces corrected with local CAR (blue; see Methods). **b**, Impact transient magnitudes for all 4 probe options chronically implanted with external referencing, and corrected with global or local CAR (n=6 trials, one animal, median±interquartile range). Probes with unity gain buffer amplifiers at the sites (Opt. 2 & 4) offer no significant advantage for CAR-processed data over probes without buffers (Opt. 1 & 3). **c**, Transients as in **a,** induced by chewing food, and **d**, comparison of all 4 options as in **b**. Same trial counts, one animal. Again, there was no significant advantage to buffer amplifiers after CAR correction (two-sample t-test, P=0.1266, α=0.05, one-tailed). The median and interquartile ranges are computed from 12 chewing events measured at 270 sites (Opt. 4) or 374 sites (Opts. 1, 2, & 3). *n* in **b** and **d** represents the number of independent samples (number of sites x number of trials). See Methods for details.

Extended Data Figure 3. Light sensitivity tests. a,b, A comparison of the light sensitivity of active and passive *Neuropixels* probes, along with "conventional" Si probes**. a**, Plot of transient amplitude vs. illumination power density for a 5 ms directly-applied 473nm light pulse. Active sites, especially unswitched were most sensitive. Switched and unswitched passive probes were much less sensitive. In each measurement a 5 ms light pulse was applied singly or in a pulse train at 20 Hz for 1 sec. **b,** Example response to illumination with a 5 ms pulse at the indicated power density. In all cases, probes were illuminated with light from a 100 µm core multimode fiber with the probe immersed in 1X phosphate buffered saline. Below intensities of 10-20 mW/mm^2 directly onto the probe, there is no impact on spike detection (see Extended Data Figure 8) or LFP phase or magnitude determination for passive switched *Neuropixels* probes. Experiments in **a,b** were performed once for each probe type. **c-e**, *Neuropixels* recording sites were immersed in saline and directly illuminated with blue (465 nm) LED light from a 200 micron diameter, 0.66 NA fiber optic cable. Light was delivered with 6 different pulse shapes (ramp, raised cosine, square 1 ms, 10 ms, 100 ms, and 1 s) at 3 peak power levels. **c**, Light power measured with an amplified photodetector for all 18 pulse types. **d,e,** Artifacts on a representative channel for low (cyan traces), middle (magenta traces), and high (yellow traces) light levels. For reference, the input range of the LFP band (gain of 250x) is overlaid across the LFP plots.

Extended Data Figure 4 Long-term stability studies: Effects of shank width, TiN sites, and active and switched sites. a-d, To compare the chronic performance of 50 µm wide and 70 µm wide shanks as well as TiN and PEDOT-coated gold sites, 4-shank probes with 2 shanks of each width were fabricated. One version had PEDOT-coated gold sites and a second had TiN sites. These were tested in separate animals. **a**, A diagram of the probe geometry for both probes, two of 4 shanks, a photograph of the distal end of a TiN site shank, and an electron microscopy image of one TiN site. The site is 12×12 µm. These probes were chronically implanted in rat medial prefrontal cortex (mPFC) and recorded in unrestrained animals, without advancing the electrodes, in multiple sessions over a period of 6-8 weeks (further implantation, recording, and analysis details are described in the Methods). **b**, The event rate vs implant age for one of two rats with TiN probes in mPFC. We define an event as time-coincident spikes recorded on a contiguous group of sites for which the maximum amplitude on any site in the group exceeds the threshold. **c**, The event rate vs implant age for four rats with one probe each in mPFC: two animals with TiN site probes, two animals with Gold:PEDOT site probes. Differences in behavioral state likely contribute to the variability in event rate. **d**, The event SNR, defined in the Methods. The stability of this signal quality metric suggests that the drop in event rate for PEDOT-1 was due to biological factors unrelated to probe site integrity. **e-g**, Probes (Phase 2) of all four shank designs, passive, active, passive switched, and active switched were implanted chronically in rat mPFC. Recordings were made at least once per week. Data analysis, implant method, and recording procedures are described in detail in the supplementary text. There is no apparent downward trend in neural activity by either metric (**e,f**), thus all four shank technologies can achieve exceptional chronic stability. **g**, mPFC recording, 200 ms of activity traces and examples of waveforms from two sorted units. Insets: Dark lines show average waveform overlaid with 30 randomly selected single event waveforms of a neuron located at the top (green) and bottom (red) of the most distal group of 128 sites.

Extended Data Figure 5. Stability of chronically implanted Phase 3 active and switched probe technologies in rats. **a,b,** Phase 3 fully integrated probes: two of four designs were implanted in mPFC of rats as for Phase 2 (Extended Data Figure 4). One probe with amplified sites and two switchable, un-amplified probes (the preferred technology) were implanted. Amplified, switchable probes were implanted but were damaged electronically before adequate recording data could be accumulated. There was no indication of activity loss over the 8 weeks of recording (linear regression t-test, one-tailed, P>0.1) except for the top half of one probe (blue). This good performance was expected based on Phase 2 results, but the active and active switched probes are 70 µm wide in Phase 3 compared to 50 µm wide for Phase 2. See supplementary text for details of data analysis, implant method, and recording procedures. We define an event as time-coincident spikes recorded on a contiguous group of sites for which the maximum amplitude on any site in the group exceeds the threshold. Across a population of 14 probes chronically implanted in rat mPFC (Phases 2 and 3), we did not observe degradation of spiking activity over 8 weeks (linear regression t-test, single-tailed, P>0.1, n=30 sessions). The sole exception to this observation is shown in **a** and **b** above (blue). In this case, the upper half of the distal most 3.8 mm array lost nearly all activity over the first 30 days while the lower ~1.9 mm remained stable for the duration of the 8

weeks monitored. A few probe implants became detached from the skull after many months (3 of 16 implants, 223-482 days) or surgery wound irritation required the subject animal to be euthanized (but always after >20 weeks). **c,** mPFC recording, 200 ms of activity traces and examples of waveforms from two sorted units. Insets: Dark lines show average waveform overlaid with 30 randomly selected single event waveforms of a neuron located at the top (blue) and bottom (red) of the distal most group of 384 sites.

Extended Data Figure 6. Further examples of LFP data quality. a, Two example periods of LFP data, over the entire depth of the probe. The data were filtered with a third-order Butterworth low-pass filter with 300 Hz cutoff frequency, but otherwise unprocessed. Only one channel from each depth along the probe is shown, so the total number of plotted traces is 192 rather than 384. Left example shows an epoch without ripples, and right example shows an epoch with a ripple (indicated by red arrow). The ripple is expanded in the inset. **b**, Quantification of LFP signal amplitude (root mean square) across depth. At right, the anatomical locations of the sections of the probe are depicted, which were determined from histology, part of which is shown in panel **c**, along with functional markers such as spike rates and amplitudes. **c**, Histological section depicting the location of the probe (stained with DiI) as it passed through hippocampus. **d**, Theta-filtered LFP. The same data from panel **a** (left) were filtered with a third-order bandpass Butterworth filter between 4 and 10 Hz, and are here depicted as a colormap to emphasize the phase inversion at the CA1 pyramidal layer (indicated by red dashed line).

Extended Data Figure 7. Spike band signal quality across brain areas and multiple acute recordings. a, For each channel in each brain area, the number of neurons with a mean waveform >20μV was counted ('density'). **b**, For each neuron recorded in each brain area, the number of channels on which that neuron produces a mean waveform >20 μV ('spread') was counted.In a separate set of experiments, the same probe was used for a series of 12 acute *in vivo* recordings in 10 animals across 4 months. **c**, The signal quality of each recording was computed by measuring the amplitude of detected spikes relative to the detection threshold within a 30 second selection of the recording. The detection threshold used was always 5 times the standard deviation (σ) of the mean signal. **d**, The mean (+/- SEM, n=200) ratio of the 90th percentile (blue), 50th percentile (red) and 10th percentile (green) to the 5σ detection threshold across all channels with an event, for each recording.

Extended Data Figure 8. Recording during optogenetic stimulation of excitatory and inhibitory cell populations. a,b, A *Neuropixels* probe was inserted into primary visual cortex of a Rorb-Cre;Ai32 mouse expressing ChR2 in Rorb-positive cells, which are primarily excitatory neurons of layer 4. Stimulation was carried out with a 465 nm LED coupled to a 200 micron, 0.66 NA fiber optic cable placed on the surface of the cortex approximately 1 mm from the recording site. Each trial (N = 20) consisted of a raised cosine light pulse 1 s in duration, with a peak intensity of 300 mW/mm^2. **a**, Average multiunit firing rate across 250 channels, aligned to the start of the optogenetic stimulus. Location of the brain surface is marked with a white line. **b**, Average LFP band response to the optogenetic stimulus for 125 channels along the left edge of the probe (a subset of the sites in panel **a**). **c,d,** A *Neuropixels* probe was inserted into primary visual cortex of a PV-Cre;Ai32 mouse expressing ChR2 in PV-positive cells, which are primarily fast-spiking inhibitory neurons. Stimulation was carried out with a 470 nm laser focused to a ~150 μm diameter spot on the surface of the cortex at the recording site. Each trial (N = 15) consisted of a 500 ms, 40 Hz raised cosine light pulse, with a peak intensity of 25 mW/mm^2. **c**, Average multiunit firing rate (regular-spiking waveforms only) across 150 channels, aligned to the start of the optogenetic stimulus. Location of the brain surface is marked with a white line. **d**, Average LFP band response to the optogenetic stimulus for 75 channels along the left edge of the probe (a subset of the sites in panel **c**). **e-i,** Light artifact and detection of optogenetically driven spikes in a PV-Cre;Ai32 mouse. **e,** Raw data for a single trial with optical transients at onset and offset of light stimulation. **f,** The same trial and channel as **e**, after the light-evoked transient was reduced by subtraction of the median of the activity across all channels as in Extended Data Figure 1. Spike times identified by the spike sorting algorithm are indicated with circles below the trace. **g,** Zoomed in view of the period of light stimulation. **h,** The average number of spikes, for this unit, during light stimulation. Each bin is 1.7 msec. **i,** Overlaid waveforms for 3 spikes during light stimulation (blue) and outside of light stimulation (black).

Extended Data Figure 9. Stability of a probe implanted chronically in a mouse over 21 weeks. a, A chronically implanted mouse, 85 days after probe implantation. The subject was a male C57Bl/6J mouse, 92 days old at the time of probe implant. The probe is protected by a custom plastic enclosure. Total implant weight was ~3.0 g, including the metal headplate (bar with side holes) that was used to fix the head during recordings. **b,** Firing rate across the probe, measured by counting spikes with amplitude >50 μV trough-to-peak at each depth as a function of days since implantation. Day 0 was recorded in the anesthetized condition during implantation; all subsequent days were recorded during wakefulness. **c,** Total summed firing rate across all channels, showing a decrease in the few days after implantation followed by mostly stable high-yield recordings for a period of 153 days, after which time the experiment was ended by experimenter decision. **d,** Example waveforms from three putative frontal cortical neurons and one neuron in the lateral septal nucleus recorded on day 153 after implantation. Probe icon at right depicts the location of the waveforms on the probe.